

Universal phase transition and band structures for spinless nodal-line and Weyl semimetals

Ryo Okugawa¹ and Shuichi Murakami^{1,2}

¹*Department of Physics, Tokyo Institute of Technology,
2-12-1 Ookayama, Meguro-ku, Tokyo 152-8551, Japan*

²*TIES, Tokyo Institute of Technology, 2-12-1 Ookayama, Meguro-ku, Tokyo 152-8551, Japan*

(Dated: October 10, 2018)

We study a general phase transition between spinless topological nodal-line semimetal and Weyl semimetal phases. We classify topological nodal lines into two types based on their positions and shapes, and their phase transitions depends on their types. We show that a topological nodal-line semimetal becomes the Weyl semimetal by breaking time-reversal symmetry when the nodal lines enclose time-reversal invariant momenta (type-A nodal lines). We also discuss an effect of crystallographic symmetries determining the band structure of the topological nodal-line semimetals. Thanks to protection by the symmetries, the topological nodal-line semimetals can transition into spinless Weyl semimetals or maintain the nodal lines in many crystals after inversion symmetry is broken.

PACS numbers: 73.20.At, 73.43.Nq

I. INTRODUCTION

Many topological semimetals are realized by strong spin-orbit interactions leading to the gap closing. One example of the topological semimetals is a Weyl semimetal (WSM)^{1,2}. The WSMs have three-dimensional nondegenerate Dirac cones. The gapless points called Weyl nodes are protected by the topology in the momentum space, and necessarily appear in pairs. The WSMs also show topological surface states called Fermi arcs²⁻⁵. As another example, topological Dirac semimetals have been also investigated⁶⁻⁹. The topological Dirac semimetals can be obtained in systems with time-reversal (TR) and inversion (I) symmetries, and have Dirac nodes with fourfold degeneracy. Moreover, recent works propose new topological semimetals whose band crossings lie on symmetry points with high-dimensional irreducible representations¹⁰⁻¹³.

On the other hand, a novel topological semimetal appears in spinless systems with TR- and I symmetries. It is called a topological nodal line (TNL) semimetal (SM). The TNLSMs have twofold degenerate nodal lines on general points in the three-dimensional Brillouin zone. (If spin degeneracy is considered, the TNLs are fourfold degenerate.) The line degeneracy is accidental, and characterized by a quantized Berry phase equal to π ^{14,15}. Hence, the nodal lines are protected topologically. However, existence of characteristic surface states called drumhead surface states is not necessarily guaranteed^{9,16}. The TNLSMs have been predicted theoretically in various materials with negligible spin-orbit interaction. The candidates are carbon allotropes¹⁷⁻¹⁹, $\text{Cu}_3(\text{Pd}, \text{Zn})\text{N}$ ^{20,21}, Ca_3P_2 ^{22,23}, LaN ²⁴, compressed black phosphorus²⁵, alkaline-earth metals^{16,26}, BaSn_2 ²⁷, and CaP_3 family²⁸. DC conductivities are calculated in hyperhoneycomb lattices with the TNLs^{29,30}. Recently, ZrSiS has been observed as a TNLSM experimentally³¹⁻³⁵.

Meanwhile, one can find another type of spinless

nodal lines protected by mirror or glide symmetry but not topology. The nodal lines lie on the mirror/glide plane. The spinless nodal-line semimetals have been reported in CaAgP and CaAgAs , which are noncentrosymmetric^{36,37}. In general, the protection by the mirror symmetry can coexist with the topological protection. Actually, the nodal lines in ZrSiS are protected also by the glide symmetry^{31,32}.

We can also realize the WSM phase in spinless systems when either TR or I symmetry is absent³⁸⁻⁴¹. The spinless WSM phase has been realized experimentally in a photonic crystal^{42,43}. Some spinless WSM phases appear between topologically trivial and nontrivial insulator phases characterized by some crystal symmetries^{44,45}. In some models, the spinless WSM is expected to be driven from the nodal-line semimetal by a circularly polarized light⁴⁶⁻⁵¹.

Yet the purely spinless TNLSMs and the spinless WSMs have not been discovered experimentally in three-dimensional electronic systems. Additionally, the topological nodal-bands are suggested in non-electronic systems which do not have spin-orbit interactions^{40,52-58}. Therefore, it is important to give a general framework of a phase transition between the spinless topological semimetal phases, as studied in spinful systems^{1,8,59}. Moreover, it is recently shown that band evolutions of spinful WSMs are determined by crystallographic symmetries, although the Weyl nodes may arise at generic points⁶⁰. Extending this theory to the TNLSMs helps us to understand the band structures easily.

In this work, we study a generic topological phase transition between the spinless semimetal phases. To elucidate the phase transition, we classify TNLs into two types, type-A and type-B. The type-A and type-B TNLs are distinguished by their locations and shapes, which roughly corresponds to whether or not the TNLs enclose a time-reversal invariant momentum. We show that depending on the type of the TNL, its topological na-

ture and its evolution under symmetry-breaking perturbations are quite varied. It is shown that the type-A TNLSM phase always becomes the spinless WSM phase when the TR symmetry is broken. Furthermore, we show how other crystallographic symmetries constrain positions of the TNLs in the type-A TNLSMs. As a result, even if the I symmetry is broken, the system remains in a nontrivial topological semimetal phase by the crystal symmetries in many cases. We also demonstrate the phase transition between the TNLSM phase and the WSM phase by using a lattice model to confirm our theory.

This paper is organized as follows. We classify the topological nodal line into the type-A and the type-B TNLSMs and show corresponding effective models in Sec. II. In Sec. III, we show general phase transitions in TNLSMs when the TR or I symmetry is broken. We elucidate effects of other crystal symmetries on band structures and nodal lines of the topological semimetals in Sec. IV. In Sec. V, we discuss phase transitions in TNLSMs with additional crystallographic symmetries, when the TR or I symmetry is broken. Our results are summarized in Sec. VI.

II. CLASSIFICATION OF TNLSMS INTO TWO TYPES

In this section we classify TNLs into two types: type-A and type-B. We consider systems with I and TR symmetries, whose operators are denoted by P and Θ , respectively. Θ is a complex conjugation operator K . These symmetries give constraints $H(-\mathbf{k}) = PH(\mathbf{k})P^{-1} = \Theta H(\mathbf{k})\Theta^{-1}$, where $H(\mathbf{k})$ is the Hamiltonian. Because of these symmetries, it is important to describe behaviors of the energy bands at a time-reversal invariant momentum (TRIM).

We classify TNLs based on their shapes around one of the TRIM. Because of the TR symmetry, TNLs appear symmetrically with respect to TRIM. When there are more than one TNL in the Brillouin zone, we consider each TNL separately. It may sometimes happen that a single TNL is not time-reversal invariant in itself, i.e. it is not symmetric with respect to the TRIM considered; in such cases, we consider instead a pair of TNLs which is symmetric with respect to the TRIM, as shown in Fig. 1(b). Obviously, this pairing of TNLs is independent of the choice of the TRIM. It may also happen that some TNLs may traverse across the Brillouin zone, like an ‘‘open orbit’’ of an electron under a magnetic field within semiclassical theory. Our theory also works in such cases.

To classify individual TNLs, we first define a TR-invariant plane, as a plane in \mathbf{k} space containing the TRIM considered. This plane is invariant under the TR symmetry. Since the TNL are symmetric with respect to the TRIM, the TNL always intersects with the TR-invariant plane $2(2N+1)$ or $4N$ times, where N is a

non-negative integer (Fig. 1). If the TNL intersects with the TR-invariant plane $2(2N+1)$ times, the TNL encloses the TRIM as shown in Fig. 1(a), and we call the TNL a type-A TNL. On the other hand, if the number of the intersection points is $4N$, we call the TNL a type-B TNL as shown in Fig. 1(b). If the TNLs are tangential to the TR-invariant plane, we slightly move the TR-invariant plane to eliminate the points of tangency, and count the number of intersections. This classification is independent of the choice of the TR-invariant plane for the fixed choice of the TRIM. Furthermore, it is also independent of the choice of the TRIM, which can be directly shown by considering a TR-invariant plane containing more than one TRIM.

In the following, we construct a two-band effective Hamiltonian consisting of the conduction and the valence bands around the TRIM, in order to facilitate our understanding of the behaviors of the TNLs. To construct an effective Hamiltonian we assume that each TNL is isolated, meaning that we can take a vicinity of the TRIM which contain only one TNL. First, we consider the case where the parity eigenvalues of the conduction and the valence bands are different at the TRIM, and are inverted from the other TRIM. As we see later, this corresponds to the type-A TNL. Then the I symmetry is given by $P = \pm\sigma_z$, where $\sigma_{i=x,y,z}$ denote Pauli matrices acting on the space spanned by the conduction and the valence bands. Then, from the TR- and I symmetries, the effective Hamiltonian is

$$H_{\text{TNL}}(\mathbf{q}) = a_y(\mathbf{q})\sigma_y + a_z(\mathbf{q})\sigma_z, \quad (1)$$

where \mathbf{q} is a wavevector measured from the TRIM, $a_y(-\mathbf{q}) = -a_y(\mathbf{q})$, and $a_z(-\mathbf{q}) = a_z(\mathbf{q})$. Therefore, the TNL is represented by $a_y(\mathbf{q}) = 0$ and $a_z(\mathbf{q}) = 0$. Here, we are considering the case where the parities of the bands at the TRIM are inverted from those at other TRIM. Therefore, the coefficient $a_z(\mathbf{q})$ changes sign as we go away from the TRIM ($\mathbf{q} = 0$). Hence, the equation $a_z(\mathbf{q}) = 0$ defines a closed surface encircling the TRIM, and together with the other condition $a_y(\mathbf{q}) = 0$, it indeed defines a TNL enclosing the TRIM, corresponding to the type-A TNL. In this case, a sign of a parameter m defined by $m \equiv a_z(\mathbf{q} = 0)$ describes whether the bands are inverted or not. Suppose we start from the TNLSM phase and change this parameter m across zero. As m approaches zero, the nodal line shrinks. At $m = 0$ the gap closes at the TRIM ($\mathbf{q} = 0$), and then the gap opens.

In addition, some of the type-B TNLs can also be described by Eq. (1). It happens when the sign of $a_z(\mathbf{q})$ at $\mathbf{q} = 0$ and that away from $\mathbf{q} = 0$ are the same, whereas $a_z(\mathbf{q})$ vanishes at some \mathbf{q} . This corresponds to the type-B TNL, by counting the number of intersections between the TNL and the TR-invariant plane.

Second, when the parity eigenvalues of the conduction and the valence bands are identical at the TRIM, $P = \pm\sigma_0$ and the effective Hamiltonian is

$$H_{\text{TNL}}(\mathbf{q}) = a_x(\mathbf{q})\sigma_x + a_z(\mathbf{q})\sigma_z, \quad (2)$$

where $a_x(-\mathbf{q}) = a_x(\mathbf{q})$ and $a_z(-\mathbf{q}) = a_z(\mathbf{q})$. TNLs exist if $a_x(\mathbf{q}) = 0$ and $a_z(\mathbf{q}) = 0$. It is straightforward to see that the number of intersections between the TNL and the TR-invariant plane is $4N$ (N : integer), meaning that this TNL is of type B. Unlike Eq. (1), the gap closing at the TRIM is prohibited by level repulsion. Meanwhile, as we explained later, the TNL can be annihilated without crossing the TRIM.

In some cases, there are more than one TNLs in the Brillouin zone. Ca (calcium) has four type-A TNLs and Yb (ytterbium) without the spin-orbit coupling has six pairs of type-B TNLs¹⁶. Let n_A and n_B denote the number of type-A TNLs and that of type-B TNLs, respectively. Then one can relate these numbers with the \mathbb{Z}_2 topological invariants ν_i ($i = 0, 1, 2, 3$) introduced in Ref. 20. The topological invariants are defined as

$$(-1)^{\nu_0} = \prod_{n_j=0,1} \prod_m^{\text{occ.}} \xi_m(\Gamma_{n_1 n_2 n_3}), \quad (3)$$

$$(-1)^{\nu_i} = \prod_{n_i=1, n_j \neq i=0,1} \prod_m^{\text{occ.}} \xi_m(\Gamma_{n_1 n_2 n_3}), \quad (4)$$

where $\xi_m(\Gamma_{n_1 n_2 n_3})$ is a parity eigenvalue of the m -th occupied band at a TRIM $\Gamma_{n_1 n_2 n_3} = (n_1 \mathbf{G}_1 + n_2 \mathbf{G}_2 + n_3 \mathbf{G}_3)/2$, $n_i = 0, 1$. $\mathbf{G}_{i=1,2,3}$ are reciprocal vectors. These topological invariants determine whether the number of intersections between the TNLs and a half of an arbitrary plane including four TRIM is even or odd²⁰. In particular, it directly follows from Ref. 20 that

$$\nu_0 \equiv n_A \pmod{2}. \quad (5)$$

For example, both in Ca and Yb (without the spin-orbit coupling), the \mathbb{Z}_2 topological numbers are trivial, i.e. $(\nu_0; \nu_1 \nu_2 \nu_3) = (0; 000)$ ¹⁶, and it agrees with the number of TNLs, $(n_A, n_B) = (4, 0)$ in Ca and $(n_A, n_B) = (0, 6)$ in Yb.

Next we consider an evolution of a TNL under continuous deformation of the system. A TNL may change its shape under the deformation, and sometimes the number of intersections with a TR-invariant plane may change. We first note that as long as the TNL does not go across the TRIM, the number of intersections between a TNL and a TR-invariant plane can change only by an integer multiple of four, because the TNL remains symmetric with respect to the TRIM. Therefore, a type-B TNL can shrink and be annihilated without crossing the TRIM, because $4N \equiv 0 \pmod{4}$. On the other hand, to annihilate a type-A TNL, it should go across the TRIM, and thereby the gap closes at the TRIM. From the argument of the \mathbb{Z}_2 topological numbers, in order to annihilate a type-A TNL, the \mathbb{Z}_2 topological number should change, and thus this gap closing should necessarily accompany an exchange of the parity eigenvalues at the TRIM between the valence and the conduction bands. This agrees with the argument in Eq. (1). If the two bands forming the TNL have the same parity eigenvalues, the gap closing at the TRIM is not allowed because

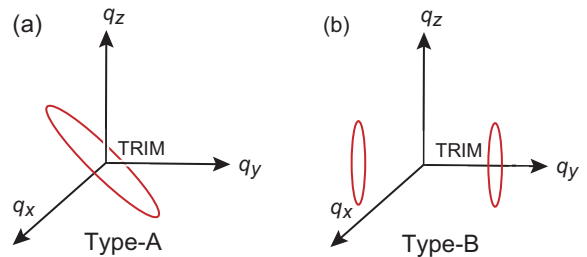


FIG. 1. Schematic drawing of (a) type-A and (b) type-B TNLs. (a) When a type-A TNL encloses the TRIM, the type-A TNL intersects with any of the TR-invariant planes including the TRIM $2(2N + 1)$ times. (b) A type-B TNL intersects with the TR-invariant plane $4N$ times.

of the level repulsion. Meanwhile, when the bands have opposite parity eigenvalues, there are no constraints for gap-closing points. We remark that one can change the numbers of type-A TNLs and type-B TNLs under continuous deformation of the system without changing the topological invariant ν_0 . For example, one can continuously deform from the TNLs in Ca to those in Yb via Lifshitz transitions, without changing ν_0 .

III. PHASE TRANSITION INVOLVING TNLMS

To elucidate phase transitions involving the TNLMS phase, we add symmetry-breaking perturbations to the system. We use the effective Hamiltonians for the TNLMSs described by Eqs. (1) and (2). We assume that the TNLs are realized before breaking the symmetry, and let ℓ denote the TNL. On the TNLs, $a_y(\mathbf{q}) = a_z(\mathbf{q}) = 0$ in Eq. (1) or $a_x(\mathbf{q}) = a_z(\mathbf{q}) = 0$ in Eq. (2) holds. In this section, we ignore crystallographic symmetries other than I symmetry.

A. Type-A TNLMSs with TR breaking

Firstly, we break the TR symmetry in type-A TNLMSs. The allowed perturbation term is $a_x(\mathbf{q})\sigma_x$ which satisfies $a_x(-\mathbf{q}) = -a_x(\mathbf{q})$ because of the I symmetry. We can assume that the perturbation is so small that the coefficients of Eq. (1) remain zero on ℓ after the TR breaking. Thus, the gap closes when $a_x(\mathbf{q}) = 0$, $\exists \mathbf{q} \subset \ell$ in the presence of the small TR breaking term. In fact, such wavevectors satisfying $a_x(\mathbf{q}) = 0$ always exist somewhere on ℓ because $a_x(\mathbf{q})$ is an odd function of \mathbf{q} and the type-A TNL ℓ encloses the TRIM represented by $\mathbf{q} = 0$. The emergent gapless points are Weyl nodes [Fig. 2 (a)]. The Weyl nodes appear symmetrically with respect to the TRIM, and the minimal number of Weyl nodes is two. The two Weyl nodes are related by the I symmetry, and thus have opposite monopole charges. Hence, when the TR symmetry is broken, the system changes from the

type-A TNLSM phase to the spinless WSM phase.

We also show another proof of the appearance of the spinless WSM phase by breaking the TR symmetry based on a topological description. We assume that a type-A TNL encloses a TRIM Γ , and that the energy bands are gapless only on the TNL. We consider a TR-invariant plane P_{Γ} which includes Γ . The TR-invariant plane has $2(2N+1)$ intersection points $\pm\mathbf{k}_i (i = 1, \dots, 2N+1)$ with the type-A TNL. We focus on pairs of the gapless points on P_{Γ} , which are related by the I symmetry. Because the closings of the gap at these gapless points are protected topologically by the TR- and I symmetries, the bands generally become gapped at these points when we weakly break the TR symmetry. The perturbation terms obtained in each pair $\pm\mathbf{k}_i$ have opposite signs, because of the I symmetry. Thus, the bands at each pair of wavevectors $\pm\mathbf{k}_i$ contribute by $+1$ or -1 to the Chern number defined on the plane P_{Γ} ⁶¹. By summing over all the $(2N+1)$ pairs, the Chern number on the plane P_{Γ} is nonzero. On the other hand, we introduce another plane $P_{\Gamma\parallel}$ which is parallel to P_{Γ} , but does not intersect nodal lines [Fig. 2 (b)]. By assumption, the Chern number defined on $P_{\Gamma\parallel}$ is zero before introducing the perturbation. As long as the perturbation is small, the band gap does not close on the plane $P_{\Gamma\parallel}$, and the Chern number remains zero on $P_{\Gamma\parallel}$ after the TR symmetry is broken. Therefore, the Chern numbers are different between P_{Γ} and $P_{\Gamma\parallel}$, and it means that between P_{Γ} and $P_{\Gamma\parallel}$ the energy bands should have gapless points, i.e. Weyl nodes. As a consequence, the WSM phase necessarily emerges from the type-A TNLSM phase by breaking the TR symmetry.

B. Type-A TNLSMs with I breaking

Secondly, we introduce a term which weakly breaks the I symmetry but preserves the TR symmetry in type-A TNLSMs. The allowed term is described by $a_x(\mathbf{q})$ which satisfies $a_x(-\mathbf{q}) = a_x(\mathbf{q})$. Then, $a_x(\mathbf{q})$ can be nonzero on the whole loop ℓ since $a_x(\mathbf{q})$ is an even function of \mathbf{q} . Therefore, the energy bands can become gapped. It is natural from the viewpoint of topology; because the perturbation terms obtained in each pair $\pm\mathbf{k}_i$ have the same signs, the Chern number on the plane P_{Γ} is zero,

implying that there appear no gapless points in general.

C. Type-B TNLSMs with TR or I breaking

Next, we study a phase transition of the type-B TNLSM phase by breaking the TR- or I symmetry. The additional perturbation term for Eq. (1) and (2) for breaking either of the TR- or I symmetries is $a_x(\mathbf{q})\sigma_x$ and $a_y(\mathbf{q})\sigma_y$, respectively. Now the perturbation is generally nonzero everywhere on ℓ , whichever symmetry is broken. Even if the perturbation term is an odd function of \mathbf{q} , it can be nonzero on ℓ because the type-B TNLs do not enclose the TRIM, unlike the type-A TNLs. Therefore, in general, by breaking the TR- or I symmetry, a gap opens, and the WSM phase does not appear from the type-B TNLSM phase.

D. Phase transition in a lattice model

In this subsection, we see a phase transition from the type-A TNLSM phase to the spinless WSM phase by using a lattice model, and we see agreement with the discussion in Sec. IIIA. We use a model on a diamond lattice given by

$$H = \sum_{\langle ij \rangle} t_{ij} c_i^\dagger c_j + \sum_{\ll ij \gg} t'_{ij} c_i^\dagger c_j. \quad (6)$$

The first term represents nearest-neighbor hoppings between the sublattices A and B. Here, we denote the three translation vectors by $\mathbf{t}_1 = \frac{a}{2}(0, 1, 1)$, $\mathbf{t}_2 = \frac{a}{2}(1, 0, 1)$, and $\mathbf{t}_3 = \frac{a}{2}(1, 1, 0)$, where a is a lattice constant. Then, the four nearest-neighbor bonds are $\boldsymbol{\tau} = \frac{a}{4}(1, 1, 1)$, and $\boldsymbol{\delta}_{i=1,2,3} = \boldsymbol{\tau} - \mathbf{t}_{i=1,2,3}$. We express the hoppings in the direction of $\boldsymbol{\delta}$ as subscripts. For example, the hoppings in the direction of $\boldsymbol{\tau}$ and $\boldsymbol{\delta}_{i=1,2,3}$ are written by $t_{\boldsymbol{\tau}}$ and $t_{\boldsymbol{\delta}_{i=1,2,3}}$, respectively. The second term represents the next nearest-neighbor hoppings. The twelve next nearest-neighbor bonds are represented by $\pm\mathbf{t}_{i=1,2,3}$, and $\pm\mathbf{u}_{i=1,2,3}$, where $\mathbf{u}_1 = \mathbf{t}_3 - \mathbf{t}_2$, $\mathbf{u}_2 = \mathbf{t}_3 - \mathbf{t}_1$, and $\mathbf{u}_3 = \mathbf{t}_1 - \mathbf{t}_2$. In addition, we denote the next nearest-neighbor hoppings between the same sublattices A(B) by $t_{\boldsymbol{\delta}}^{A(B)}$. When the system is I-symmetric, $t_{\boldsymbol{\tau}}$ and $t_{\boldsymbol{\delta}_{i=1,2,3}}$ are real, and $t_{\boldsymbol{\delta}}^A = (t_{\boldsymbol{\delta}}^B)^*$. The Hamiltonian in the momentum space is

$$H(\mathbf{k}) = \left[2 \sum_{\mathbf{d}} \text{Re}[t_{\mathbf{d}}^A] \cos \mathbf{k} \cdot \mathbf{d} \right] \sigma_0 + \left[t_{\boldsymbol{\tau}} + \sum_i t_{\boldsymbol{\delta}_i} \cos \mathbf{k} \cdot \mathbf{t}_i \right] \sigma_x + \left[\sum_i t_{\boldsymbol{\delta}_i} \sin \mathbf{k} \cdot \mathbf{t}_i \right] \sigma_y + \left[2 \sum_{\mathbf{d}} \text{Im}[t_{\mathbf{d}}^A] \sin \mathbf{k} \cdot \mathbf{d} \right] \sigma_z, \quad (7)$$

where \mathbf{d} in the sum runs over $\mathbf{t}_{i=1,2,3}$ and $\mathbf{u}_{i=1,2,3}$. The Pauli matrices $\sigma_{i=0,x,y,z}$ act on the sublattice degree of

freedom. In this model, the parity operator is represented by $P = \sigma_x$. Then, the parity eigenvalues ξ of the

occupied bands at the TRIM $\Gamma_{n_1 n_2 n_3}$ are given by

$$\xi(\Gamma_{n_1 n_2 n_3}) = -\text{sgn} \left[t_\tau + \sum_i t_{\delta_i} (-1)^{n_i} \right]. \quad (8)$$

The topological invariant ν_0 is obtained from $(-1)^{\nu_0} = \prod_{n_j=0,1} \xi(\Gamma_{n_1 n_2 n_3})$.

When $t_{\delta}^{A(B)}$ are real i.e. $\text{Im}[t_{\delta}^A] = 0$, the model has TR symmetry, which case has been studied in Ref. 62. In Ref. 62, it is shown that the energy bands can have a type-A TNL around the TRIM $\Gamma_{111} = L = \frac{\pi}{a}(1, 1, 1)$. The type-A TNL exists when the parity eigenvalue $\xi(\Gamma_{111})$ is opposite from those at the other TRIM. To realize it, we set $t_\tau/t_{\delta_1} = 1.4$, $t_{\delta_2}/t_{\delta_1} = 1.1$, and $t_{\delta_3}/t_{\delta_1} = 0.9$. We also assume that all the second nearest neighbor hoppings are identical, having the values $t_{\delta}^A/t_{\delta_1} = 0.1$. Since all the nearest-neighbor hoppings are different and real, the model has only TR- and I symmetries. Then, the type-A TNL appears around the L point as seen in Fig. 2 (c), which is as expected from our argument in Sec. IIIA.

Next we break the TR symmetry by adding finite imaginary parts of t_{δ}^A . For example, this TR breaking can be included as Peierls phases from magnetization. We put $t_{\mathbf{d}}^A = t e^{i\phi}$ for the next nearest-neighbor hoppings represented by $\mathbf{d} = \mathbf{t}_{i=1,2,3}$ and $\mathbf{u}_{i=1,2,3}$, where t and ϕ are real constants. Then, $t_{\mathbf{d}}^A = t e^{-i\phi}$ when $\mathbf{d} = -\mathbf{t}_{i=1,2,3}$ and $\mathbf{d} = -\mathbf{u}_{i=1,2,3}$. In order to break the TR symmetry, we put $t/t_{\delta_1} = 0.1$ and $\phi = 0.1$ for instance. Consequently, we find that a topological phase transition occurs from the type-A TNL phase to the spinless WSM phase. Figure 2 (c) shows the two Weyl nodes which emerge from the type-A TNL.

Instead of the TR-breaking, we can break the I symmetry by adding an on-site staggered potential given by $H_{IB} = M_s \sum_i \lambda_i c_i^\dagger c_i$, where λ_i takes values $+1$ for the A sublattices and -1 for the B sublattices. Then, we can directly see that the type-A TNL becomes gapped.

IV. CRYSTAL SYMMETRIES AND BAND STRUCTURES OF TYPE-A TNLMS

In Sec. III, we have discussed the TNLMSs by considering only TR- and I symmetries. In this section, we also take account into twofold rotational (C_2) and mirror (M) symmetries, because $C_2 M$ is equal to the space inversion. Particularly, we show how the two symmetries, C_2 and M , constrain band structures having type-A TNLs.

A. Band structures of the type-A TNLMSs

Now, we classify the type-A TNLs into two cases according to whether or not the TRIM which the TNLs enclose is invariant under C_2 and M symmetries. Because $P = C_2 M$, in I-symmetric systems, a little group of the TRIM often contains C_2 and M symmetries in pairs. If

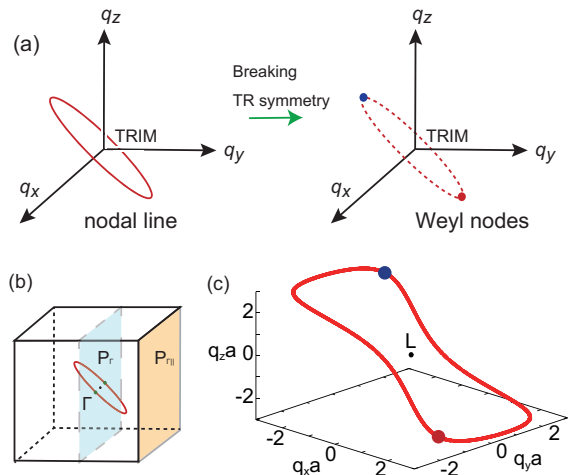


FIG. 2. (a) Schematic drawing of the band evolution. The red solid line is the TNL around the TRIM. The blue and the red points are the spinless Weyl nodes left on the loop ℓ (red dashed line). The difference between colors of the Weyl nodes corresponds to opposite monopole charges. (b) Schematic drawing of the type-A TNL and the time-reversal invariant planes. The red line is the type-A TNL. The blue and orange regions represent P_\perp and P_\parallel , respectively. The green dots are the intersection points of the type-A TNL and P_Γ . (c) Change of the band structure from the type-A TNL to the spinless Weyl nodes in a lattice model. The axes represent wavevectors measured from the point L . The red loop is the type-A TNL around the L point when $t_\tau/t_{\delta_1} = 1.4$, $t_{\delta_2}/t_{\delta_1} = 1.1$, $t_{\delta_3}/t_{\delta_1} = 0.9$, and $t/t_{\delta_1} = 0.1$. The blue and red dots are the Weyl nodes which appear from the type-A TNL for the finite TR breaking $\phi = 0.1$.

the TRIM is not invariant under the two symmetries, we call this case (I). When the TRIM considered is invariant under C_2 and M , we call the case (II). Here, twofold screw symmetries and glide symmetries can be treated similarly to C_2 and M symmetries, respectively, and the systems with these symmetries can be included in the case (II), except for some special cases at the Brillouin zone boundary for nonsymmorphic space groups (see the Appendix A). Actually, the case (II) is more important for application to real materials because 89 space groups of all the 92 space groups with I symmetry have the two symmetries⁶³.

In fact, the band structures and the phase transition of the type-A TNLMSs for (I) have already been studied in Sec. II and III, because there is no additional symmetry which further constrains the phase transition. For example, CaP_3 ²⁸ is included in the case (I).

In the case (II), the two symmetries C_2 and M give some constraints to the effective Hamiltonian described by Eq. (1). Since the parity eigenvalues are different for the conduction and the valence bands of the type-A TNLs, either of the C_2 or the M symmetry has different eigenvalues for the conduction and the valence bands. In spinless systems, eigenvalues of the C_2 and the M symmetries take values ± 1 . Then, because $P = M C_2$, there

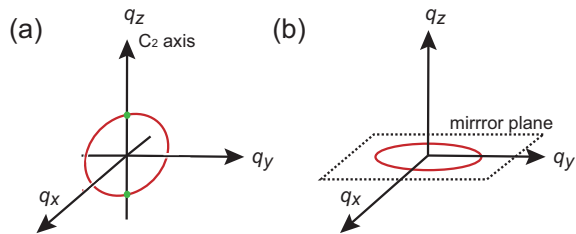


FIG. 3. Schematic positions of the nodal lines in the type-A TNL around the TRIM. (a) The type-A TNL for the case (i) has the intersection points with the C_2 invariant axis, which are indicated by the green dots. (b) For the case (ii), the type-A TNL appears on the mirror-invariant plane.

are two cases for combinations of eigenvalues C_2 and M at the TRIM; (II)-(i) eigenvalues of M are the same and those of C_2 are different, and (II)-(ii) eigenvalues of M are different and those of C_2 are the same. They correspond to two different matrix representations: (II)-(i) $M = \pm\sigma_0$ and $C_2 = \pm\sigma_z$, and (II)-(ii) $M = \pm\sigma_z$ and $C_2 = \pm\sigma_0$. We can calculate the band structures for these cases, and the details are shown in the Appendix A. The resulting positions of the nodal lines are shown in Fig. 3, where we set the twofold rotational axis and the mirror plane to be the z axis and xy plane, respectively. For (II)-(i), as seen in Fig. 3 (a), the type-A TNL encircles the TRIM and intersects the C_2 -invariant axis. The TNL is symmetric with respect to the mirror plane $q_z = 0$. For (II)-(ii), the type-A TNL appears on the mirror-invariant plane as shown in Fig. 3 (b).

B. Applications of the theory of the band structures to the candidate materials of TNLsMs

The results in the previous subsection can be easily generalized to little groups with many different pairs of C_2 and M symmetries. We apply the theory to several candidates of the type-A TNLsMs. First, we consider fcc Ca, whose space group is No. 225¹⁶. Ca have four type-A TNLs near each of the four TRIM L . The little group at the L points is D_{3d} which contains three C_2 -rotational operations. The two bands forming the TNLs belong to A_{1g} and A_{2u} states at the point L , and they have different C_2 eigenvalues. Therefore, the TNLs in Ca intersect the L - W lines, which are the C_2 invariant axes but do not lie on mirror planes, in accordance with our theory.

Next, we apply this theory to $\text{Cu}_3\text{ZnN}^{20}$. The space group of Cu_3ZnN is No. 221. The energy bands have type-A TNLs around the three TRIM X , whose little groups are D_{4h} . The type-A TNLs are formed by A_{2u} and A_{1g} states at the X points. The D_{4h} group contains a fourfold-rotational (C_4) operation, four C_2 operations whose rotational axes are normal to the principal axis, and the corresponding five mirror operations. Then, the A_{2u} and A_{1g} states have opposite eigenvalues of the four

C_2 symmetries. Thus, the TNLs cross the X - M lines and X - R lines, which are the C_2 -invariant axes. Meanwhile, the two states have the same eigenvalues of the C_4 symmetry. Hence, $C_4 = \sigma_0$ leads to different eigenvalues of the mirror symmetry $M = P(C_4)^2 = \sigma_z$. Therefore, the TNLs also appear on the mirror-invariant plane normal to the C_4 -invariant axis. As a result, the type-A TNLs in Cu_3ZnN not only cross the C_2 -invariant axes but also exist on the mirror plane.

Last, we remark that the type-A TNLs are predicted to appear on the mirror planes in many candidates such as $\text{Cu}_3(\text{Pd}, \text{Zn})\text{N}^{20,21}$, $\text{Ca}_3\text{P}_2^{22,23}$, LaN^{24} , and compressed black phosphorus²⁵. They belong to (II)-(ii) and the existence of TNLs is understood from the difference in eigenvalues of M between the conduction and valence bands.

V. PHASE TRANSITIONS OF TYPE-A TNLsMs AND CRYSTAL SYMMETRIES

In this section, we show that for type-A TNLsMs in the case (II), the presence of C_2 and M symmetries changes phase transitions when we break TR- or I symmetry.

A. Type-A TNLs protected by crystal symmetries with TR breaking

Here, we break the TR symmetry in the type-A TNL. When energy bands cross on high-symmetry lines or planes, and have different eigenvalues of crystal symmetries, the band crossing is protected by the symmetries, the band crossing is protected by the symmetries. Therefore, such degeneracy remains on high-symmetry lines or planes, even when the TR symmetry is broken. Therefore, in the case (II)-(i), where the type-A TNL crosses the C_2 -invariant axis, the TR breaking creates Weyl nodes on the C_2 -invariant axis as shown in Fig. 4. In the effective model, the protection originates from the fact that the perturbation $a_x(0, 0, q_z)$ always vanishes on the C_2 axis.

Next, in the case (II)-(ii), where the type-A TNL is always on the mirror-invariant plane, the nodal line remains on the mirror plane even without the TR symmetry. In the effective 2×2 model, it is seen from the fact that the perturbation $a_x(q_x, q_y, 0)$ vanishes on the mirror plane. In particular, one needs to break the M symmetry in order to realize the WSM phase.

B. Type-A TNLs protected by crystal symmetries with I breaking

We study effects of the I breaking for the case (II) in this subsection. In the case (II), where the system has C_2 and M symmetries, violation of the I symmetry is equivalent to breaking either C_2 or M symmetry because $P = MC_2$. Therefore, the topological semimetal phases

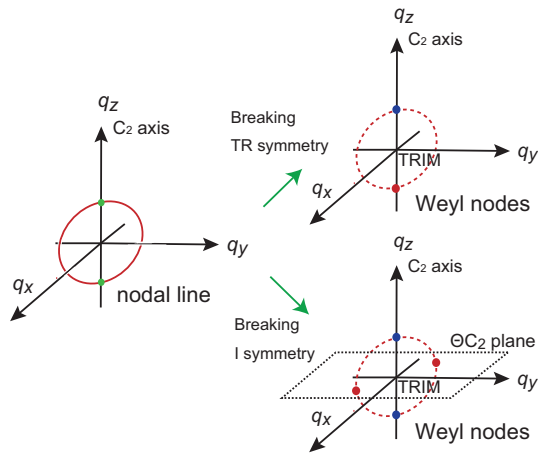


FIG. 4. Realization of the spinless Weyl nodes by breaking the TR or the I symmetry in the case (II). The blue and the red points represent the Weyl nodes. If the TR symmetry is broken, the Weyl nodes appear on the C_2 invariant axis. When the I symmetry is broken, we obtain a pair of Weyl nodes on the C_2 -invariant axis and another pair on the ΘC_2 -invariant plane.

may survive in a different way between (II)-(i) and (II)-(ii).

First, we consider the case (II)-(i). When the type-A TNL intersects C_2 -invariant axes, the system becomes a spinless WSM phase by breaking the I symmetry while retaining the C_2 symmetries. Then, we obtain Weyl nodes not only on the C_2 invariant axes but also on the ΘC_2 -invariant plane ($q_z = 0$), because of the symmetry protection. In the effective model, $\Theta C_2 = K\sigma_z$ symmetry leads to $a_x(q_x, q_y, 0) = 0$, meaning that the perturbation is absent on this ΘC_2 -invariant plane. Here, within each pair of nodes related by the TR symmetry, monopole charges are the same. The four nodes correspond to the minimal number of Weyl nodes in TR-invariant WSMs¹. In fact, the appearance of four Weyl nodes can be understood by expanding the I-breaking perturbation term proportional to σ_x . The term expanded near the TRIM to the lowest order is $a_x(\mathbf{q}) = (\alpha q_x + \beta q_y)q_z$. Therefore, we can see that the Weyl nodes appear when either $q_z = 0$ or $q_x = q_y = 0$ is satisfied, giving the four Weyl nodes.

On the other hand, for the case (II)-(ii) of the type-A TNLs on the mirror plane. if we leave the M symmetry and break the C_2 symmetry, the nodal line survives because of the M symmetry. The mirror symmetry protects the nodal lines regardless of existence of the I symmetry. Hence, even if the I symmetry is broken, the nodal line remains unless the mirror symmetry is broken.

VI. CONCLUSION AND DISCUSSION

In the present paper, we study phase transitions and band evolutions of topological nodal-line semimetals. We

classified topological nodal-line semimetals into type-A and type-B in order to describe general phase transitions by breaking time-reversal or inversion symmetry. This classification is based on the geometrical positions of the nodal lines, and we give effective Hamiltonians for each case for analysis of symmetry breaking. The results show that the topological nodal lines enclosing a TRIM (type-A topological nodal lines) always become Weyl nodes when the time-reversal symmetry is broken. However, breaking of inversion symmetry opens a band gap in the type-A topological nodal-line semimetals, and it is confirmed by our calculation on the lattice model. On the other hand, it is shown that the type-B topological nodal lines, which do not enclose a TRIM, become gapped by breaking time-reversal symmetry. The two types are distinguishable from the shapes of the topological nodal lines.

We also showed how band structures of type-A topological nodal lines are determined by the little group at the TRIM. When the topological nodal line encircles the TRIM, which is invariant under C_2 and M symmetries of the system, they cross the C_2 -invariant axis and/or appear on the mirror-invariant plane, and consequently are protected by the symmetries. Therefore, the nodal lines or points survive in some cases, even when the time-reversal or the inversion symmetries is broken. The revealed properties are also useful to search spinless topological semimetals in many materials because many space groups with I symmetry have various C_2 and M symmetries. As a result, the spinless WSMs can be predicted in many candidates of the topological nodal-line semimetals protected by the C_2 symmetries when we break the I symmetry.

Our study tells us how to realize a spinless WSM phase. In electronic systems, the spinless WSM phase appear from the type-A topological nodal-line semimetal phases not only by a circularly polarized light⁴⁶⁻⁵¹ but also by magnetic ordering, an external electric field, structural transition, and so on. Moreover, our theory can be applied to spinless fermions in cold atoms and bosonic bands. The experiments have potential in bosonic metamaterials of photons and phonons where lattice structure and its symmetry are flexibly controllable.

The TNLs may cross each other, and our classification into type-A and type-B still works for the TNLs with mutual crossings. Meanwhile, in the presence of crossings, the effective models become different from those discussed in our paper, which is beyond the scope of this paper. In this context, classification of possible patterns of their crossings and their evolution under the spin-orbit coupling was studied recently in Ref. 64. In Ref. 64 only the TNLs based on the mirror symmetry are discussed, and the main focus is on the crossings of the TNLs. Meanwhile our paper includes both the TNLs from the mirror symmetry and those from the π Berry phase, and therefore the target of our research is different from that of Ref. 64.

ACKNOWLEDGMENTS

This work was supported by JSPS KAKENHI Grant Numbers 16J08552 and 26287062 and by MEXT Elements Strategy Initiative to Form Core Research Center (TIES).

Appendix A: Classification of the type-A TNLs and their band structures

We have classified type-A TNLs into the two cases (I) and (II) in Sec. IV. The classification provides information on band evolutions and phase transitions involving type-A TNLs. In this appendix, we explain band structures of type-A TNLs in the two cases (I) and (II). The type-A TNLs are formed by two bands with opposite parity eigenvalues at the TRIM, and they can be described by the two-band effective Hamiltonian by Eq. (1). Here, to describe the TNLs by the two-band effective Hamiltonian, we assume that the TNLs are formed only by two nondegenerate states. In fact, a similar two-band effective Hamiltonian has been used in spinful WSMs in order to describe band evolutions in Ref. 60, and therefore, here we can extend the analysis in Ref. 60 to some of the spinless TNLs as well. In Ref. 60, it is shown that when two bands touch each other on high-symmetry lines or planes, emergent gapless nodes evolve along the lines and the planes where the two bands have the different eigenvalues. By using these results, we can understand band structures of type-A TNLs.

For example, in Sec. IV we introduced two cases (II)-(i) and (ii) for type-A TNLs, formed by two bands with C_2 and M symmetry. These two cases are classified according to the C_2 and M eigenvalues at the TRIM, and the effective Hamiltonian for the two cases are constrained by these two symmetries. For simplicity, we set the C_2 axis and the M plane to be the z axis and xy plane, respectively. From the constraints, we obtain $\sigma_z H_{\text{TNL}}(-q_x, -q_y, q_z) \sigma_z = H_{\text{TNL}}(q_x, q_y, q_z)$ in the case (II)-(i). Meanwhile, in the case (II)-(ii), we obtain $\sigma_z H_{\text{TNL}}(q_x, q_y, -q_z) \sigma_z = H_{\text{TNL}}(q_x, q_y, q_z)$. Although eigenvalues of the C_2 and M symmetries are different in spinless and spinful systems, the expressions for these constraints are the same both in spinless and in spinful

cases⁶⁰. As a result, the type-A TNL of the case (II)-(i) crosses the C_2 axis while the type-A TNL of the case (II)-(ii) appears on the M plane, both in spinless and in spinful systems. In some cases, several type-A TNLs can enclose the same TRIM if a little group at the TRIM contains some C_2 and M symmetries.

There are various options for the little group at the TRIM, which affects the position of the type-A TNLs. (I) refers to the case where the TRIM is neither C_2 - nor M -symmetric. Therefore, the little group is C_i or C_{3i} . In this case (I), the type-A TNL does not necessarily cross high-symmetry lines. For example, if the two bands have the same C_3 eigenvalues at the TRIM whose little group is C_{3i} , the type-A TNL lies at a general position.

(II) refers to the case where the TRIM is C_2 - and M -symmetric. In this case, as we have shown in Sec. IV, the type-A TNLs necessarily cross the high-symmetry lines or appear on the mirror-invariant planes, thanks to symmetry protection. The little groups can also have rotational symmetries besides the C_2 symmetry. When the conduction and the valence bands belong to different subspaces of the C_n -rotational symmetries, the type-A TNLs can intersect the high-symmetry lines. On the other hand, when the two bands belong to different subspaces of the mirror symmetry, the type-A TNLs are on the mirror-invariant plane. In particular, if the eigenvalues of the C_4 or C_6 symmetry are the same, the type-A TNL exists on the mirror-invariant plane perpendicular to the C_4 - or C_6 -invariant axes because $(C_4)^2 = C_2$ and $(C_6)^3 = C_2$.

Here we comment on TNLs in systems with a nonsymmorphic space group having twofold screw (S_2) symmetries or glide (G) symmetries. Inside the Brillouin zone, the TNLs are similar to those with a symmorphic space group, because there is no extra degeneracy due to nonsymmorphic symmetry together with TR symmetry. Meanwhile, S_2 and G symmetries may give rise to extra degeneracy on the Brillouin zone boundary by TR symmetry, if the square of the symmetry operations becomes -1 . For example, by combination of several G symmetries and the TR symmetry, spinless nodal lines can contain fourfold-degenerate points at the TRIM on the surface of the Brillouin zone⁶⁵. As another example, a nodal surface appears on the ΘS_2 -invariant plane on the surface of the Brillouin zone⁶⁶. Such cases are beyond the scope of this paper because the band crossing cannot be described by the two-band effective Hamiltonian.

¹ S. Murakami, New Journal of Physics **9**, 356 (2007).

² X. Wan, A. M. Turner, A. Vishwanath, and S. Y. Savrasov, Phys. Rev. B **83**, 205101 (2011).

³ T. Ojanen, Phys. Rev. B **87**, 245112 (2013).

⁴ R. Okugawa and S. Murakami, Phys. Rev. B **89**, 235315 (2014).

⁵ F. Haldane, arXiv:1401.0529 (2014).

⁶ Z. Wang, Y. Sun, X.-Q. Chen, C. Franchini,

G. Xu, H. Weng, X. Dai, and Z. Fang, Phys. Rev. B **85**, 195320 (2012).

⁷ Z. Wang, H. Weng, Q. Wu, X. Dai, and Z. Fang, Phys. Rev. B **88**, 125427 (2013).

⁸ B.-J. Yang and N. Nagaosa, Nature communications **5**, 4898 (2014).

⁹ C. Fang, Y. Chen, H.-Y. Kee, and L. Fu, Phys. Rev. B **92**, 081201 (2015).

- ¹⁰ B. J. Wieder, Y. Kim, A. M. Rappe, and C. L. Kane, *Phys. Rev. Lett.* **116**, 186402 (2016).
- ¹¹ Z. Zhu, G. W. Winkler, Q. S. Wu, J. Li, and A. A. Soluyanov, *Phys. Rev. X* **6**, 031003 (2016).
- ¹² H. Weng, C. Fang, Z. Fang, and X. Dai, *Phys. Rev. B* **93**, 241202 (2016).
- ¹³ B. Bradlyn, J. Cano, Z. Wang, M. Vergniory, C. Felser, R. Cava, and B. A. Bernevig, *Science* **353** (2016).
- ¹⁴ G. P. Mikitik and Y. V. Sharlai, *Phys. Rev. Lett.* **82**, 2147 (1999).
- ¹⁵ T. T. Heikkilä and G. E. Volovik, *New Journal of Physics* **17**, 093019 (2015).
- ¹⁶ M. Hirayama, R. Okugawa, T. Miyake, and S. Murakami, *Nature Communications* **8**, 14022 (2017).
- ¹⁷ Y. Chen, Y. Xie, S. A. Yang, H. Pan, F. Zhang, M. L. Cohen, and S. Zhang, *Nano letters* **15**, 6974 (2015).
- ¹⁸ H. Weng, Y. Liang, Q. Xu, R. Yu, Z. Fang, X. Dai, and Y. Kawazoe, *Phys. Rev. B* **92**, 045108 (2015).
- ¹⁹ J.-T. Wang, H. Weng, S. Nie, Z. Fang, Y. Kawazoe, and C. Chen, *Phys. Rev. Lett.* **116**, 195501 (2016).
- ²⁰ Y. Kim, B. J. Wieder, C. L. Kane, and A. M. Rappe, *Phys. Rev. Lett.* **115**, 036806 (2015).
- ²¹ R. Yu, H. Weng, Z. Fang, X. Dai, and X. Hu, *Phys. Rev. Lett.* **115**, 036807 (2015).
- ²² L. S. Xie, L. M. Schoop, E. M. Seibel, Q. D. Gibson, W. Xie, and R. J. Cava, *APL Mater.* **3**, 083602 (2015).
- ²³ Y.-H. Chan, C.-K. Chiu, M. Y. Chou, and A. P. Schnyder, *Phys. Rev. B* **93**, 205132 (2016).
- ²⁴ M. Zeng, C. Fang, G. Chang, Y.-A. Chen, T. Hsieh, A. Bansil, H. Lin, and L. Fu, arXiv:1504.03492 (2015).
- ²⁵ J. Zhao, R. Yu, H. Weng, and Z. Fang, *Phys. Rev. B* **94**, 195104 (2016).
- ²⁶ R. Li, H. Ma, X. Cheng, S. Wang, D. Li, Z. Zhang, Y. Li, and X.-Q. Chen, *Phys. Rev. Lett.* **117**, 096401 (2016).
- ²⁷ H. Huang, J. Liu, D. Vanderbilt, and W. Duan, *Phys. Rev. B* **93**, 201114 (2016).
- ²⁸ Q. Xu, R. Yu, Z. Fang, X. Dai, and H. Weng, *Phys. Rev. B* **95**, 045136 (2017).
- ²⁹ K. Mullen, B. Uchoa, and D. T. Glatzhofer, *Phys. Rev. Lett.* **115**, 026403 (2015).
- ³⁰ M. Ezawa, *Phys. Rev. Lett.* **116**, 127202 (2016).
- ³¹ L. M. Schoop, M. N. Ali, C. Straßer, A. Topp, A. Varykhalov, D. Marchenko, V. Duppel, S. S. Parkin, B. V. Lotsch, and C. R. Ast, *Nature communications* **7** (2016).
- ³² M. Neupane, I. Belopolski, M. M. Hosen, D. S. Sanchez, R. Sankar, M. Szlowska, S.-Y. Xu, K. Dimitri, N. Dhakal, P. Maldonado, P. M. Oppeneer, D. Kaczorowski, F. Chou, M. Z. Hasan, and T. Durakiewicz, *Phys. Rev. B* **93**, 201104 (2016).
- ³³ J. Hu, Z. Tang, J. Liu, X. Liu, Y. Zhu, D. Graf, K. Myhro, S. Tran, C. N. Lau, J. Wei, and Z. Mao, *Phys. Rev. Lett.* **117**, 016602 (2016).
- ³⁴ X. Wang, X. Pan, M. Gao, J. Yu, J. Jiang, J. Zhang, H. Zuo, M. Zhang, Z. Wei, W. Niu, *et al.*, *Advanced Electronic Materials* **2**, 1600228 (2016).
- ³⁵ R. Singha, A. K. Pariari, B. Satpati, and P. Mandal, *Proceedings of the National Academy of Sciences* **114**, 2468 (2017).
- ³⁶ A. Yamakage, Y. Yamakawa, Y. Tanaka, and Y. Okamoto, *Journal of the Physical Society of Japan* **85**, 013708 (2016).
- ³⁷ Y. Okamoto, T. Inohara, A. Yamakage, Y. Yamakawa, and K. Takenaka, *Journal of the Physical Society of Japan* **85**, 123701 (2016).
- ³⁸ J. L. Mañes, *Phys. Rev. B* **85**, 155118 (2012).
- ³⁹ C. Fang, M. J. Gilbert, X. Dai, and B. A. Bernevig, *Phys. Rev. Lett.* **108**, 266802 (2012).
- ⁴⁰ L. Lu, L. Fu, J. D. Joannopoulos, and M. Soljačić, *Nature photonics* **7**, 294 (2013).
- ⁴¹ J.-Y. Zou and B.-G. Liu, *Phys. Rev. B* **93**, 205435 (2016).
- ⁴² L. Lu, Z. Wang, D. Ye, L. Ran, L. Fu, J. D. Joannopoulos, and M. Soljačić, *Science* **349**, 622 (2015).
- ⁴³ W.-J. Chen, M. Xiao, and C. T. Chan, *Nature communications* **7** (2016).
- ⁴⁴ A. Alexandradinata, C. Fang, M. J. Gilbert, and B. A. Bernevig, *Phys. Rev. Lett.* **113**, 116403 (2014).
- ⁴⁵ H. Kim and S. Murakami, *Phys. Rev. B* **93**, 195138 (2016).
- ⁴⁶ A. Narayan, *Phys. Rev. B* **94**, 041409 (2016).
- ⁴⁷ Z. Yan and Z. Wang, *Phys. Rev. Lett.* **117**, 087402 (2016).
- ⁴⁸ C.-K. Chan, Y.-T. Oh, J. H. Han, and P. A. Lee, *Phys. Rev. B* **94**, 121106 (2016).
- ⁴⁹ K. Taguchi, D.-H. Xu, A. Yamakage, and K. T. Law, *Phys. Rev. B* **94**, 155206 (2016).
- ⁵⁰ M. Ezawa, *Phys. Rev. B* **96**, 041205 (2017).
- ⁵¹ Z. Yan and Z. Wang, *Phys. Rev. B* **96**, 041206 (2017).
- ⁵² M. Xiao, W.-J. Chen, W.-Y. He, and C. T. Chan, *Nature Physics* **11**, 920 (2015).
- ⁵³ W. Gao, B. Yang, M. Lawrence, F. Fang, B. Béri, and S. Zhang, *Nature Communications* **7**, 12435 (2016).
- ⁵⁴ D. Z. Rocklin, B. G. Chen, M. Falk, V. Vitelli, and T. C. Lubensky, *Phys. Rev. Lett.* **116**, 135503 (2016).
- ⁵⁵ Z. Yang and B. Zhang, *Phys. Rev. Lett.* **117**, 224301 (2016).
- ⁵⁶ F.-Y. Li, Y.-D. Li, Y. B. Kim, L. Balents, Y. Yu, and G. Chen, *Nature Communications* **7**, 12691 (2016).
- ⁵⁷ A. Mook, J. Henk, and I. Mertig, *Phys. Rev. Lett.* **117**, 157204 (2016).
- ⁵⁸ A. Mook, J. Henk, and I. Mertig, *Phys. Rev. B* **95**, 014418 (2017).
- ⁵⁹ S. Murakami and S.-i. Kuga, *Phys. Rev. B* **78**, 165313 (2008).
- ⁶⁰ S. Murakami, M. Hirayama, R. Okugawa, and T. Miyake, *Science Advances* **3**, e1602680 (2017).
- ⁶¹ F. D. M. Haldane, *Phys. Rev. Lett.* **61**, 2015 (1988).
- ⁶² R. Takahashi and S. Murakami, *Phys. Rev. B* **88**, 235303 (2013).
- ⁶³ C. Bradley and A. Cracknell, *The mathematical theory of symmetry in solids: representation theory for point groups and space groups* (Oxford University Press, 2010).
- ⁶⁴ S. Kobayashi, Y. Yamakawa, A. Yamakage, T. Inohara, Y. Okamoto, and Y. Tanaka, *Phys. Rev. B* **95**, 245208 (2017).
- ⁶⁵ R. Takahashi, M. Hirayama, and S. Murakami, arXiv:1704.02151 (2017).
- ⁶⁶ Q.-F. Liang, J. Zhou, R. Yu, Z. Wang, and H. Weng, *Phys. Rev. B* **93**, 085427 (2016).